Chain Tilt and Surface Disorder in Lamellar Crystals. A FTIR and SAXS Study of Labeled Long Alkanes

D. Sujeewa M. de Silva,[†,‡] Xiang-bing Zeng,[†] Goran Ungar,*[,†] and Stephen J. Spells[‡]

Department of Engineering Materials, University of Sheffield, Mappin Street, Sheffield S1 3JD, U.K., and School of Science, Sheffield Hallam University, City Campus, Sheffield S1 1WB, U.K.

Received April 30, 2002; Revised Manuscript Received July 21, 2002

ABSTRACT: Small-angle X-ray scattering (SAXS) and infrared spectroscopy (IR) are employed in a study of chain tilt and disorder in solution-crystallized long alkanes $C_{198}H_{398}$ and $C_{12}D_{25}C_{192}H_{384}C_{12}HD_{24}$ in extended and once-folded conformations. The as-grown crystals have chains perpendicular to the lamellar surface, but around 90 °C they start tilting relative to the layer normal. The tilt increases gradually to reach 35° just below melting point. The end-labeled alkane allows independent IR probing of molecular disorder at the deuterated surface layer and in the hydrogenous interior of the crystals. The initially small splitting of the CD_2 bending mode doublet and the presence of a singlet component indicated a rough surface in as-grown crystals, with considerable translational disorder. The increase in splitting and decrease in absorbance of the singlet which occur on annealing at progressively higher temperatures showed a steady improvement in translational surface order, concomitant with an increase in chain tilt angle. Thus, it is concluded that the absence of tilt in as-grown crystals is not due to high surface order, as in the case of shorter odd *n*-alkanes, but rather to high nonequilibrium surface disorder with chain ends or folds protruding out of or sunk beneath the surface. It is also concluded that chain tilt only becomes necessary as the crystal surface becomes translationally more ordered and the crystal−amorphous interface sharpens. IR also demonstrated the reversible increase in conformational disorder in the surface layer with increasing temperature and an almost negligible increase in the crystal interior. The gradual change in tilt angle and the existence of noncrystallographic basal planes is interpreted in terms of translational molecular disorder at the surface. The increased central SAXS scatter during the tilting process indicates the creation of voids associated with ridge formation and corrugation of the lamellae.

Introduction

In crystalline polymers, chains are often tilted relative to the layer normal. In polyethylene this leads, for example, to the hollow pyramid shape of solution-grown single crystals.[1] Further, chain tilt is believed to be responsible for lamellar twist in melt-crystallized spherullites.[2,3] The development of tilt is associated with crystallization or annealing at elevated temperatures. Thus, in some cases single crystals of a polymer with an orthogonal or nearly orthogonal unit cell grown from solution at low temperatures are flat lamellae with chains perpendicular to the basal (001) surface.[4,5] However, when grown at a higher temperature, the crystals are hollow pyramids or chairlike.[6] X-ray diffraction results on polyethylene single crystals suggest that in some cases an initially small tilt increases upon annealing.[7] Perpendicular-chain lamellar morphology forms in cold-rolled polyethylene, but this transforms to "parquet-floor" morphology on annealing.[8] In cold-drawn fibers the meridional small-angle X-ray scattering (SAXS) maximum splits across the meridian, giving rise to a four-point pattern when the fiber is annealed;[9] this indicates tilting of layers, with the chains remaining parallel to the draw direction. Direct crystallization from the melt at high T_c normally yields lamellar crystals with tilted chains.[10,11]

In polyethylene crystallized from melt or from poorer solvents at high temperatures, {100} growth sectors prevail, and the tilt is usually 35°, since the basal plane is {201}. The {201} tilt arises when each consecutive chain along the **a**-axis is shifted by one lattice period in the chain (**c**) direction. Such tilt allows chain folds an increased surface area, by a factor of 1/(cos 35°), while maintaining the crystallographic packing of the remaining chain intact. In hollow pyramid or chair crystals grown from solution the preferred fold surface was found to be close to {314} or {312} for {110} sectors and {201} and {301} for {100} sectors.[6] Other tilt angles have also been observed: 19° tilt corresponds to {101} basal planes and 41° tilt to {502} planes.[11,12]

Chain tilt helps to alleviate the overcrowding problem at the crystal surface. In semicrystalline polyethylene it has long been recognized that the cross-sectional area required by an amorphous chain is at least twice that required by a straight crystalline chain (the "gambler's ruin" problem).[13−17] The problem of abrupt dissipation of order at the crystal−amorphous interface is resolved in flexible polymers partly by chain tilt, but to a greater part by adjacently reentrant chain folding. There appears to be a greater tendency for chain tilt in polymers with a larger density difference between the amorphous and the crystalline phase.[18] A recent simulation study by Rutledge et al.[19] has shown graphically the way that chain tilt alleviates steric overcrowding at the crystal−amorphous interface in polyethylene. It has been estimated by theoretical considerations and by simulation that the cross section of a polyethylene chain leaving the crystal increases by a factor of 2−3, depending on the method used. Recently, this ratio has been determined experimentally as 2.8 on the basis of binary phase diagrams of long-chain *n*-alkanes.[20]

† University of Sheffield.
‡ Sheffield Hallam University.
* Corresponding author: e-mail g.ungar@sheffield.ac.uk.

10.1021/ma0206669 CCC: $22.00
Published on Web 08/30/2002

There is circumstantial evidence that lower molecular weight favors crystals with perpendicular chains. Thus, it was reported that poly(vinylidene fluoride) of $M_w = 4.7 \times 10^4$ forms perpendicular chain crystals from a 0.5/99.5 blend with poly(ethyl acrylate).[5] However, crystallization of PVDF with $M_w = 2.5 \times 10^5$ under the same conditions gave hollow pyramid and chairlike crystals with tilted chains.[21] Tilt also occurs in melt-crystallized long-chain *n*-alkanes, but in crystals grown from solution using good solvents; i.e., at low T_c, the chains are perpendicular.[22,23] This applies to chain lengths between $n \cong 60$ and $n = 390$ C atoms, the latter being the longest studied and up to four times folded. As in polyethylene, the difference between solution- and melt-crystallized material has been associated with the generally lower T_c in solution crystallization.

In apparent agreement with the behavior of polyethylene and long alkanes, shorter *n*-alkanes crystallize with perpendicular chains provided that T_c is below ca. 60−70 °C.[24] This is true for odd-numbered alkanes; even-numbered alkanes display a more complex behavior due to molecular symmetry.[25] At higher temperatures in alkanes such as $C_{33}H_{68}$ a {101} tilted form is brought about through one or several discrete transitions.[26] In this case the tilt at high temperature is associated with equilibrium surface disorder (form C) and the absence of tilt at low temperature with high end group order (form A). When perpendicular-chain solution-crystallized alkanes with more than ca. 50 carbons are heated, chain tilt is introduced gradually. Up to and including $C_{94}H_{190}$, crystals melt before a tilt of 35° is reached.[22,27]

The established and widespread view can thus, crudely, be summarized as follows: low temperature and low molecular weight favor perpendicular chains, while high temperature and high molecular weight favor tilted chains. There is less consensus as to why chains tend to be perpendicular at low temperature. The prevailing opinion, based on the analogy with short alkanes, is that the crystal surface is relatively ordered and does not require the additional area that chain tilt would provide. However, it has been proposed recently that in melt-crystallized polyethylene below $T_c \cong 127$ °C chains may be initially perpendicular, with fold ordering and chain tilting occurring subsequently.[3] This has been offered as an explanation for the S profile of the lamellae as viewed along the growth (**b**) axis. In fact, the idea that chains may crystallize initially perpendicular to the lamellar surface and tilt later has been put forward in an early study on polyethylene single crystals[6] in order to explain the corrugated lamellar habits[28] and the observed 1:1 ratio of pyramidal and chairlike crystals.

The aim of the present study is to help find answers to a number of questions concerning surface order and chain tilt. First, what is the amount of surface disorder, and what part of it is equilibrium and what is nonequilibrium (trapped kinetic disorder)? Second, what is the reason for the lack of tilt at low crystallization temperatures;i.e., is it low or is it high surface disorder? Third, how can the existence of noncrystallographic basal planes such as those reported in alkanes with 50−100 C atoms be explained?

Long-chain *n*-alkanes are used as model compounds in this work. Past research on long monodisperse alkanes has been reviewed recently, along with that on other model crystalline polymers.[29] The most recent studies using monodisperse alkanes up to $C_{390}H_{782}$ have been in morphology,[30−32] lamellar structure,[33,34] and crystallization kinetics.[31,35] The methods of investigation employed in the present work are small- and wide-angle X-ray scattering (SAXS and WAXS) and infrared (FTIR) spectroscopy. The advantage of using monodisperse alkanes is in that the stem length is known accurately, being equal to either the full or one-half the chain length under the solution crystallization conditions employed.[23,36] Thus, the tilt angle can be determined easily from the SAXS long period. Furthermore, we take advantage here of a deuterium end-labeled long alkane which allows spectroscopic probing of the surface and the interior of the crystals separately.

Experimental Section

The materials used in this work are the long *n*-alkane $C_{198}H_{398}$[37] and the recently synthesized[38] deuterated alkane, $C_{12}D_{25}C_{192}H_{384}C_{12}HD_{24}$ (abbreviated $C_{216}H_{385}D_{49}$). These materials were kindly provided by Dr. G. M. Brooke of Durham University. The compounds were crystallized from 1.3% toluene solution. The crystallization temperature T_c was 73 °C (1.5 h) for once-folded chain crystals of $C_{198}H_{398}$ and 82 °C (6 h) for extended chain crystals of $C_{198}H_{398}$ and $C_{216}H_{385}D_{49}$. Crystals were filtered relatively rapidly and dried in a vacuum at 50 °C for 2 days. Samples for X-ray diffraction experiments were put in glass capillaries, while those for IR spectroscopy were lightly pressed into 5 mm diameter pellets. It was ascertained by wide-angle X-ray diffraction that the pressed pellets contained orthorhombic crystals with no detectable amount of the triclinic modification.

The shorter alkanes used as reference for IR spectroscopy were *n*-$C_{34}H_{70}$, *n*-$C_{13}D_{28}$, and *n*-$C_{36}D_{74}$. The former was purchased from Sigma-Aldrich, and the latter two were from CDN Isotopes, having 98% isotopic purity.

SAXS experiments were performed on Station 8.2 of the Daresbury Synchrotron Radiation Source. The beam was monochromatized and double-focused onto the detector having a cross section of 2 × 0.3 mm in the sample plane.[39] A high count rate quadrant multiwire detector was used, and the sample-to-detector distance was 3.1 m. The capillary with the sample was held in a modified Linkam hot stage with mica windows and temperature control within ±0.2 °C. The beam was monitored with two ionization chambers, one in front and one behind the sample. All diffractograms were corrected for uneven channel response by dividing them with the response to homogeneous radiation of ^{55}Fe. This also took care of the slice shape of the detector window, allowing the resulting curves to be treated as if recorded with a linear detector. The correction for positional nonlinearity of the detector was tested using the first 22 orders of diffraction from wet rat tail collagen. The sample-to-detector distance in detector pixel units was calibrated using polycrystalline samples of shorter orthorhombic *n*-alkanes with precisely known unit cell lengths. A curved Inel position-sensitive detector was used for simultaneous recording of wide-angle scattering (WAXS). The diffraction pattern recorded with an image plate showed only a marginal degree of preferred orientation.

Transmission FTIR measurements were made using a Mattson Galaxy 6020 spectrometer with an MCT detector. Samples were held between KBr microscope slides in a Graseby-Specac 21500 cryostat, with temperature controlled by a 10120 temperature controller. The sample space was evacuated, and the spectrometer was purged with dry air. Spectra were obtained at 1 or 2 cm^{-1} resolution using typically 200 scans. All intensities quoted are integrated absorbances.

Results

SAXS Results. SAXS diffractograms of $C_{198}H_{398}$ and $C_{216}H_{385}D_{49}$ crystals as-grown from solution at 82 °C show a series of diffraction orders of a single fundamental periodicity $L = 254$ Å and $L = 277$ Å, respec-

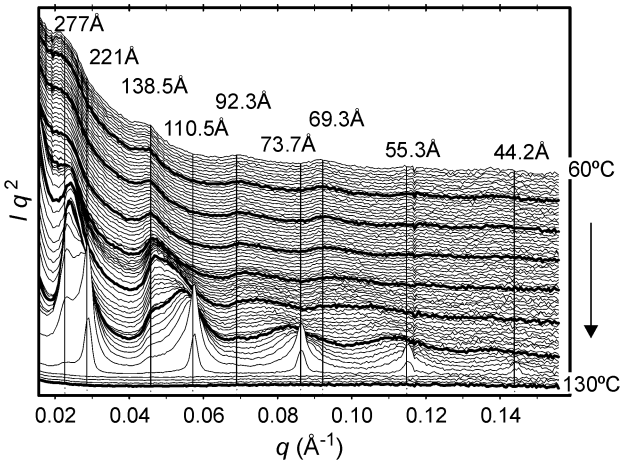

Figure 1. SAXS diffractograms of an extended-chain single-crystal mat of alkane $C_{216}H_{385}D_{49}$ during heating at 1 °C/min from 60 to 130 °C. The intensities are Lorentz corrected. Vertical grid lines, marked with the corresponding *d*-spacings, are shown at peak positions. Temperatures are indicated on the right.

tively. This matches very well the extended chain lengths of 254 and 276 Å, calculated as $1.27m + 2$,[40] where m is the carbon number. This means that, as expected from previous experience,[41] the molecular chains are extended and perpendicular to the lamellar surface. The SAXS pattern of $C_{198}H_{398}$ crystallized at 73 °C also consists of one series of diffraction orders of monotonically decreasing intensities, corresponding to a long period of 128 Å, i.e., half the chain length of the paraffin. Thus, the chains are once-folded and again normal to the lamellar plane.

A series of SAXS curves of extended-chain $C_{216}H_{385}D_{49}$ recorded during a heating run at 1 °C/min are shown in Figure 1. The diffractogram at 60 °C shows little difference from that at room temperature, and the peak positions are identical. The background increases greatly with decreasing angle, as is common in solution-crystallized polymers. This is attributed to polydisperse voids between poorly stacked lamellar packets. The discrete diffraction peaks are weak and broad in comparison with those in melt-crystallized alkanes.[42] The integral line width Θ is plotted against q^2 as diamonds in Figure 2 ($q = (4\pi \sin \theta)/\lambda$, where θ is half the scattering angle and λ is the wavelength). From the least-squares linear fit of Θ vs q^2, according to

$$\Theta = \frac{\lambda}{D} + \frac{\lambda L}{4} g^2 q^2$$

the size of coherent lamellar stacks along the lamellar normal (D) is estimated as 1300 Å, i.e., the equivalent of about 5 layers. The paracrystalline distortion factor g is 1.7%.[43] The latter parameter is defined as the relative fluctuation of the lamellar spacing, i.e.

$$g^2 = \langle (L - \langle L \rangle)^2 \rangle / \langle L \rangle^2$$

With increasing temperature, particularly above ca. 100 °C, the SAXS peaks are seen to start moving toward larger angles (Figure 1), while broadening and, in the case of the first and second order, visibly splitting. The major component is moving continuously, while a small fraction retains the original position. The latter disappears about 1 °C below the melting point, eventually leaving only a single set of sharp diffraction orders.

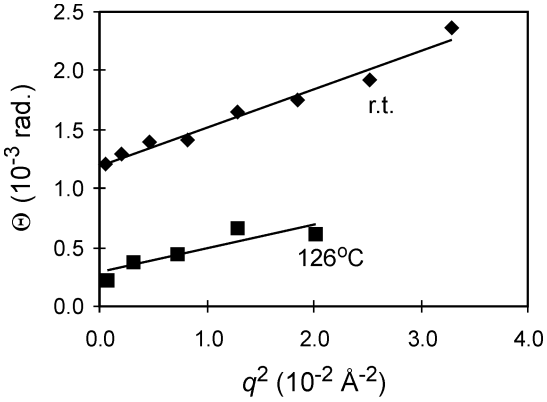

Figure 2. Line width Θ of small-angle diffraction peaks plotted against q^2 for a series of diffraction orders of extended-chain $C_{216}D_{385}D_{49}$: diamonds, as-crystallized from solution, recorded at room temperature (perpendicular form); squares, recorded at 126 °C, immediately below melting point (35° tilt).

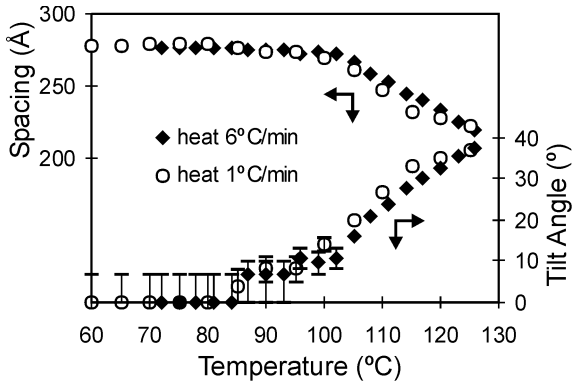

Figure 3. Temperature dependence of lamellar spacing L (upper half) and angle of chain tilt with respect to the lamellar normal (lower half) for extended-chain solution-grown crystals of $C_{216}H_{385}D_{49}$ during heating from 60 °C to the melting point. Data for heating at 1 °C/min (solid diamonds) and 6 °C/min (empty circles) are shown for comparison.

From the q^2 dependence of integral line width Θ_n of the last diffractogram before melting, the coherent domain size D is determined as 5500 Å and the distortion factor g as 1.5%.

The long spacing L for extended-chain crystals of $C_{216}H_{385}D_{49}$ is plotted against temperature in Figure 3, together with the chain tilt angle $\beta = \cos^{-1}(L/L_0)$, where L_0 is the extended chain length. The chains are seen to remain orthogonal up to $T = 85$ °C, whereupon tilt sets in and increases continuously with increasing temperature. It is only just below the melting point that β reaches 35°, the theoretical angle for {201} basal planes. The temperature dependence of the tilt angle is not affected significantly by the heating rate—compare the 1 and 6 °C/min data in Figure 3. Also, lowering the heating rate from 1 °C/min to less than 0.5 °C/h did not have a noticeable effect on the tilt angle.[44]

The behavior of extended chain crystals of alkane $C_{198}H_{398}$ on heating is very similar to that of $C_{216}H_{385}D_{49}$. The temperature dependence of L and β for $C_{198}H_{398}$ is shown in Figure 4. Here chain tilting starts at a somewhat higher temperature, but β catches up eventually and $\beta = 35°$ is reached again just before the melting point. The heating rate for the $C_{198}H_{398}$ sample was 2 °C/min, i.e., intermediate between the two rates used

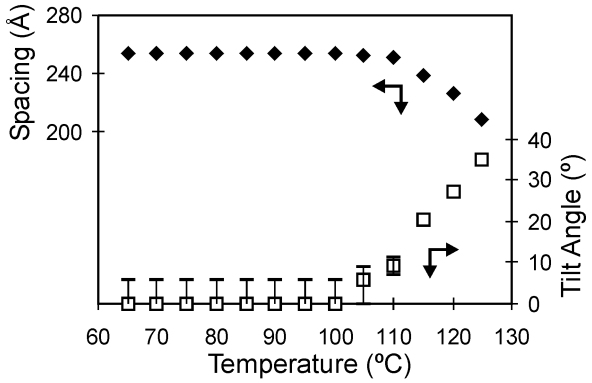

Figure 4. Temperature dependence of lamellar spacing L (solid diamonds, upper half) and angle of chain tilt (empty squares, lower half) for extended-chain solution-grown crystals of $C_{198}H_{398}$ during heating from 60 °C to the melting point at 2 °C/min.

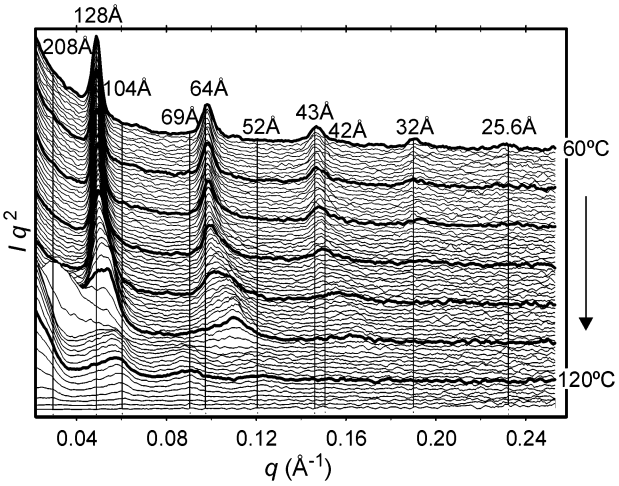

Figure 5. SAXS diffractograms of initially once-folded chain crystals of $C_{198}H_{398}$ during heating from 60 to 127 °C at 5 °C/min. The diffraction intensities are Lorentz corrected. Vertical grid lines are labeled by the corresponding d-spacings. Temperatures are shown on the right.

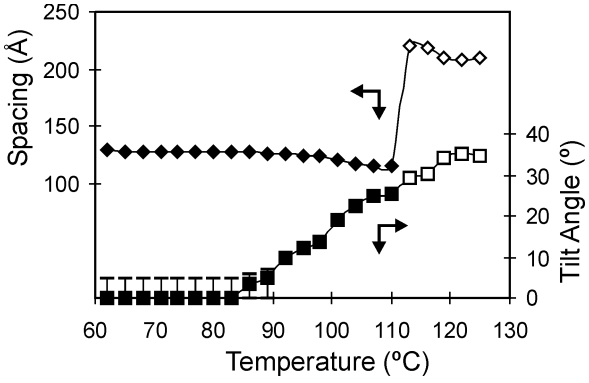

Figure 6. Temperature dependence of lamellar spacing L (diamonds, upper half) and angle of chain tilt (squares, lower half) for the initially once-folded chain solution-grown crystals of $C_{198}H_{398}$ during heating from 60 °C to the melting point at 5 °C/min. The transition from once-folded to extended form occurred between 111 and 114 °C. Solid symbols denote the once-folded and empty symbols the extended-chain form.

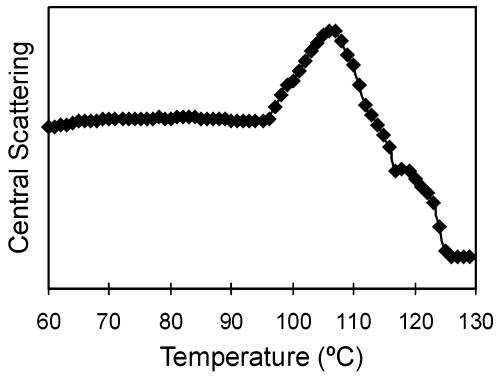

Figure 7. Relative intensity $I_{q=0.0145}$ at the arbitrarily chosen q value of 0.0145 vs temperature for the extended-chain $C_{216}H_{385}D_{49}$ single-crystal mat during heating. The intensity is representative of the continuous central scattering due to voids.

with $C_{216}H_{385}D_{49}$. As the heating rate effect can be excluded, the exact reason for the observed delay in the case of $C_{198}H_{398}$ is not clear.

The series of SAXS curves recorded during heating of $C_{198}H_{398}$ crystallized at 73 °C is shown in Figure 5. The diffractogram recorded at room temperature is very similar to that at 60 °C, the beginning of the heating run. The series of peaks is orders of the long period L = 128 Å, i.e., exactly half that for the extended chain crystals. This confirms that the alkane chains in crystals grown at 73 °C are once-folded. As with extended chain crystals, the diffraction peaks are broad. The coherent stack size D is obtained as 1600 Å (about 12 lamellar layers), and the paracrystalline distortion factor is g = 2.8%.

As temperature increases above 85 °C, the diffraction peaks from chain-folded $C_{198}H_{398}$ start moving to wider angles, showing the onset of chain tilt. In the region around 110−114 °C a transformation to extended chain crystals takes place, indicated by the doubling of L. L and β are shown in Figure 6 as a function of temperature. β had reached approximately 26° at the transition. The tilt angle continues to increase and again reaches 35° just below the melting point of extended chain crystals.

It is evident from Figures 1 and 5 that there is a drastic overall reduction in the strong diffuse central scatter as the temperature approaches the melting point. The scattered intensity $I_{q=0.0145}$ at the arbitrarily chosen q value of 0.0145, close to the central beam and sufficiently distant from any discrete peaks, is plotted against temperature in Figure 7 for extended-chain $C_{216}H_{385}D_{49}$. The drop in central scatter shows that a sintering process takes place at these temperatures, closing the voids between lamellar stacks. However, superimposed on the decrease in $I_{q=0.0145}$ is a pronounced maximum centered at 107 °C, i.e., in the middle of the chain tilting range (cf. Figure 3). An increase in central scatter is often observed during melting, caused by long-distance density fluctuations. However, that increase is much weaker than the one described here, and it occurs at or very close to the melting point, which for $C_{216}H_{385}D_{49}$ is 127.4 °C. Melting could possibly account for the shoulder in the $I_{q=0.0145}(T)$ curve at T = 120 °C.

A similar temperature dependence of the central scatter is observed for single crystals of once-folded $C_{198}H_{398}$. However, the pronounced maximum occurs here at a somewhat higher temperature and is most likely affected by the unfolding process.

An estimate of the thickness of the disordered surface layer of the crystals was made by determining σ^2, the second moment of $\Delta\eta(z)$. $\Delta\eta(z)$ is the interlayer electron density gap profile along the layer normal **z**.

$$\sigma^2 = \frac{1}{\kappa}\int z^2 \Delta\eta(z)\, dz, \quad \text{where } \kappa = \int \Delta\eta(z)\, dz$$

σ^2 was determined from the slope of the least-squares linear fit to experimental F_n vs n^2/L^2, according to the approximation[45]

$$F_n{}^2 = \kappa^2 - 4\pi^2\kappa^2 o^2(l^2/L^2) \quad \text{where } \kappa^2 = F_0{}^2$$

Here F_n is the structure factor of nth diffraction order. The above equation is of the form $I_n = C_0 + C_2 n^2$, where I_n is the corrected diffracted intensity and σ^2 is determined from C_2. We found that the experimental $I_n(n^2)$ relation for solution-grown crystals deviates from linearity, with low orders having excessive intensities. This is tentatively attributed to imperfect layer stacking and a disproportional influence of occasional wider interlamellar gaps. A fit to higher diffraction orders gave a σ^2 value of 22 Å^2 for as-grown extended-chain crystals of $C_{216}H_{385}D_{49}$ at room temperature. Approximating $\Delta\eta(z)$ with a rectangular gap profile, the full gap width D_t is obtained as 16 Å.

Since pressed mats were used in IR experiments, a simultaneous SAXS/WAXS heating run was also recorded using a portion of the same pressed mat as that used for IR. The general behavior, including tilting, was identical to that of the unpressed mat, except that the central scatter was somewhat reduced and a degree of preferred orientation was introduced. WAXS diffractograms showed only the orthorhombic reflections, with no noticeable evidence of the triclinic phase at any stage.

IR Results. Two main spectral features have been studied in this work: the crystal field splitting of methylene CH_2 and CD_2 deformation (bending) modes and the CH_2 and CD_2 wagging mode regions. In the present context, the former gives chiefly a measure of translational disorder, while the latter probes conformational disorder.

As is well-known, in crystals of polyethylene and *n*-paraffins with the orthorhombic subcell IR and Raman bands with a vibrational component in the *ab* plane are split into two components differing in frequency by $\Delta\nu$ (Davydov splitting). One component is *a*-polarized and the other *b*-polarized, depending on whether the two nonequivalent chains in the unit cell vibrate with a phase difference $\phi = 0$ or π.[46] The difference in frequency arises from the van der Waals interaction between neighboring oscillating chains. Assuming that the interoscillator interaction is proportional to their phase difference, for an infinite row of chains in a (110) plane $\Delta\nu_8 = 2\Delta\nu_0$, where $\Delta\nu_0$ is the splitting for an isolated pair of stems.[47] For an infinite stack of infinite (110) rows, i.e., an infinite crystal lamella, $\Delta\nu_{\infty\times\infty} = 2\Delta\nu_\infty = 4\Delta\nu_0$. If the domain of coupled oscillators is restricted by defects, $\Delta\nu$ decreases. A deuterated alkane chain in a hydrogenous crystal matrix, or vice versa, will decouple the oscillators and serve as a domain-limiting defect. The splitting for $j/2$ pairs of chains in a (110) row is given by

$$\Delta\nu_{j/2} = \Delta\nu_0 + (\Delta\nu_\infty - \Delta\nu_0)\sin^2\frac{(j/2-1)\pi}{j} \qquad (1)$$

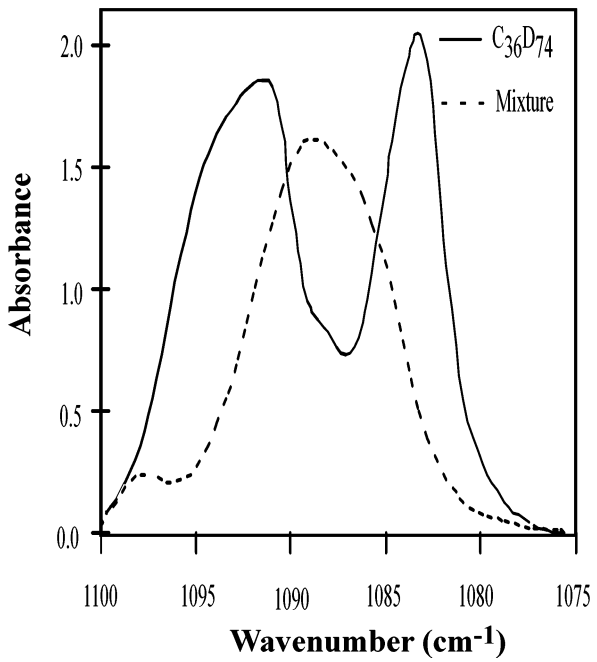

Figure 8. IR spectra in the CD_2 bending region for pure *n*-alkane $C_{36}D_{74}$ and a 1:2 w:w mixture of $C_{36}D_{74}$ and $C_{34}H_{70}$ recorded at −173 °C.

The splitting for a domain of $j \times k$ chains, i.e., for k (110) rows of j chains, can be derived by analogy as

$$\Delta\nu_{j\times k} = \Delta\nu_j + (\Delta\nu_{j\times\infty} - \Delta\nu_j)\sin^2\frac{(k-1)\pi}{2k} \qquad (2)$$

The resulting reduced band splitting $\Delta\nu_{j\times k}$ relative to $\Delta\nu_{\infty\times\infty}$ is thus a sensitive probe of local chain environment, and the mixed crystal method has been used productively in a number of studies of polymers[47−49] and paraffins.[50] Different types of defects, including thermal librations and positional and conformational defects, would all contribute to a reduction in $\Delta\nu$. Needless to say, that noncrystalline environment gives rise to a singlet, though broadened, band.

The effect of isolating deuterated chains in a 1:2 mixture of alkanes $C_{36}D_{74}$ and $C_{34}H_{70}$ on the splitting of the CD_2 bending mode at 100 K is illustrated in Figure 8. It can be seen that in pure $C_{36}D_{74}$ the band is a doublet, with $\Delta\nu = 10.1$ cm^{-1}. However, in the case of the solid solution the diluted deuterated chains produce only a broadened singlet. It should be noted that measurements at these temperatures are required in order to obtain comparable unit cell dimensions and hence doublet splittings. From experiments on perdeuterated polyethylene crystals, Cheam and Krimm give a value of $\Delta\nu_{\infty\times\infty} = 10.2$ cm^{-1} for the CD_2 bending mode.[47]

Effect of Annealing. In the case of perfectly ordered extended chain crystals of $C_{216}H_{385}D_{49}$ both the CH_2 and CD_2 deformation bands should show maximum splitting as both hydrogenous and deuterated moieties would be surrounded by their own species. The reduction in splitting of the corresponding CD_2 and CH_2 absorption bands can thus be used to probe separately the interior (hydrogenous) and the surface (deuterated) layers of the crystal. Figure 9 shows (a) the CH_2 and (b) the CD_2 deformation bands for $C_{216}H_{385}D_{49}$ crystals recorded at 100 K. Spectra are shown for the as-crystallized alkane as well as after annealing at a series of increasing

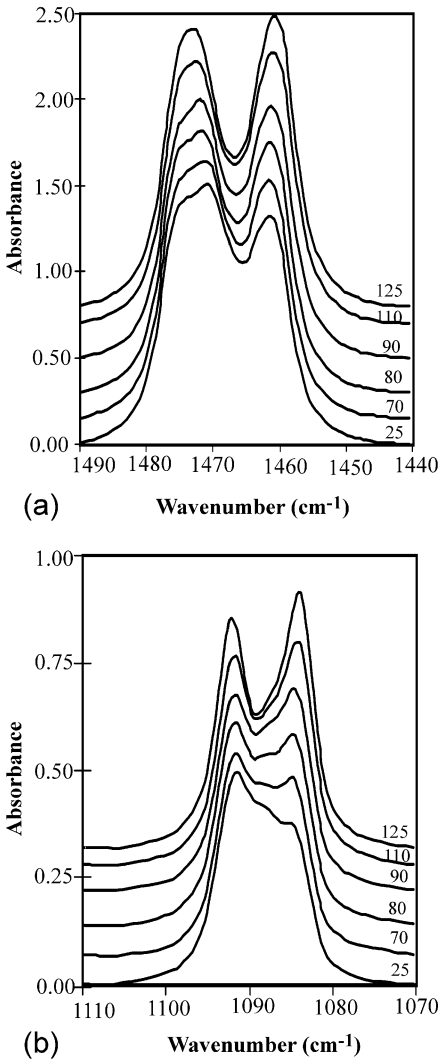

Figure 9. IR spectra in the CH_2 bending region (a) and CD_2 bending region (b) for extended-chain $C_{216}H_{385}D_{49}$ crystals as-grown from solution and annealed for 30 min at the temperatures indicated (in °C). The spectrum of unannealed crystals is labeled "25". All spectra were recorded at −173 °C.

temperatures. Annealing times were between $^1/_2$ and 1 h at each temperature. The CH_2 band from the as-grown crystals (Figure 9a) shows a large splitting which changes little on annealing. $\Delta\nu_{CH_2}$ is 13.1 cm^{-1}, which is a typical value for crystalline polyethylene and *n*-alkanes at this temperature.[47] In contrast, the two components of the CD_2 bending absorption from as-grown crystals (Figure 9b) are poorly resolved, and there is a third singlet component in the middle. The components were resolved by a combination of Fourier deconvolution and curve fitting, and $\Delta\nu$ of the two crystalline CD_2 components is shown in Figure 10 (solid circles). For the initial crystals the splitting is only 6.8 cm^{-1} as compared with 10.1 cm^{-1} for $C_{36}D_{74}$ (Figure 8) and deuterated polyethylene.[47] The reduced splitting shows that the deuterated, i.e., surface layer of the as-grown crystals, is considerably more disordered than the hydrogenous interior. The presence of the additional singlet component indicates that a sizable proportion of deuterated end groups act as isolated oscillators.[48]

Unlike the CH_2 band, the CD_2 deformation band changes substantially on annealing (see Figure 9b). Curve fitting shows that the splitting of the two crystal-

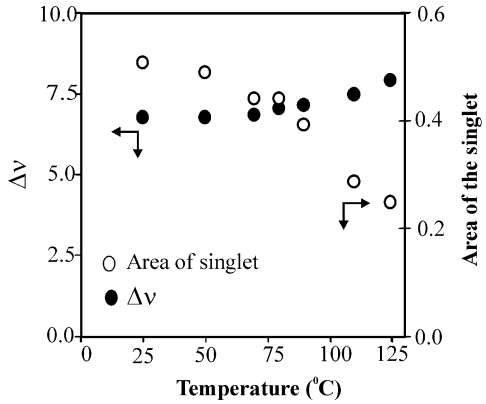

Figure 10. Magnitude of CD_2 bending mode splitting ($\Delta\nu$, solid circles) and relative area of the central singlet component for extended-chain $C_{216}H_{385}D_{49}$ crystals as a function of annealing temperature. Spectra were recorded at −173 °C (see Figure 9b). The measurements were made using a combination of Fourier deconvolution and curve fitting.

line components increases progressively from 6.8 to 7.9 cm^{-1} (Figure 10) and that the area of the intermediate singlet decreases by a half upon annealing at the highest temperature of 125 °C, which is 2 °C below the melting point. This behavior indicates that annealing results in irreversible perfecting of the surface layers of the crystal in terms of increasing the average size of ordered domains of coupled oscillators and decreasing the proportion of decoupled, i.e., translationally, orientationally, or conformationally ill-fitting terminal $C_{12}D_{25}$ groups. FTIR measurements on alkane *n*-$C_{13}H_{28}$ at 100 K showed that the orthorhombic crystalline form develops a CD_2 bending splitting of 9.4 cm^{-1}. It is therefore reasonable to suggest that the $C_{12}D_{25}$ end caps of $C_{216}H_{385}D_{49}$ are sufficiently long to produce the full $\Delta\nu_{\infty\times\infty}$ obtained for deuterated polyethylene or longer chain alkanes. Equation 2 can be used with appropriate scaling to obtain a quantitative estimate[48] of the average size of ordered deuterated clusters in as-crystallized $C_{216}H_{385}D_{49}$. These turn out to be 6−18 chains, increasing to 16−21 chains on annealing. Any departure of the deuterated end layer from the ideal vibrational model would be likely to reduce $\Delta\nu_{\infty\times\infty}$ and hence increase the calculated size of ordered domains, particularly in the case of annealed crystals where $\Delta\nu$ is close to $\Delta\nu_{\infty\times\infty}$.

After each annealing, spectra were also recorded at room temperature in order to observe any irreversible change in conformational disorder. The conformationally sensitive CH_2 and CD_2 wagging regions were investigated. Band assignments in these regions will be discussed in detail in the next section. Presently, it suffices to say that there were no noteworthy changes in the CH_2 wagging region between 1250 and 1400 cm^{-1} where bands characteristic of *gtg*, *gtg′*, and *gg* sequences are found. Thus, the number of conformational defects in the crystal interior, which is already low in as-grown crystals, does not decrease noticeably on annealing. On the other hand, some reduction in absorbance occurs in the CD_2 wagging region each side of the CH_2 band at 964 cm^{-1} (see Figure 11). Bands at 956 and 990 cm^{-1} are attributed to conformational defects in $(CD_2)_x$ chains (see below). Most of the decrease in absorbance on the right-hand side in Figure 11, associated with the 956 cm^{-1} band, had occurred already before the 110 °C annealing, whereas most of the decrease in the 990 cm^{-1} region had taken place before annealing at 121 °C.

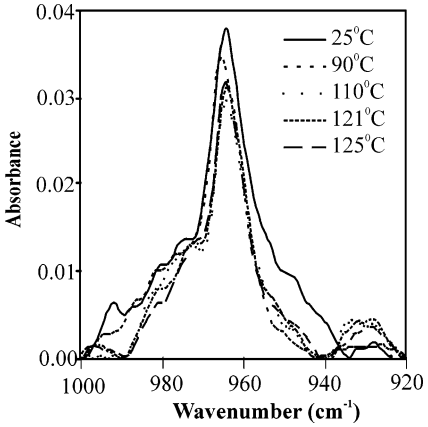

Figure 11. IR spectra of $C_{216}H_{385}D_{49}$ crystals recorded at room temperature after annealing at the temperatures indicated. A spectral region containing CD_2 wagging modes of nonplanar conformations is shown. Note the decrease in absorbance around 990 and 950 cm^{-1} caused by annealing and relatively low temperatures.

Thermoreversible Disorder. Once the crystals had been annealed at the highest temperature and thus cleared as much as possible of trapped nonequilibrium defects, we proceeded to study the temperature dependence of reversible equilibrium defects. SAXS did not show reversibility of chain tilt. Once a certain tilt angle was reached, its value being apparently determined exclusively by the maximum annealing temperature, the highest tilt attained persisted after cooling to room temperature. However, the SAXS peak intensity did in all cases show a reversible increase with temperature, which is attributed to increased density deficiency of the disordered surface layer.[22,29]

IR spectra in the range of the CD_2 and CH_2 bending modes respectively are shown in parts a and b of Figure 12 for the sample annealed at 125 °C. The spectra were recorded at a series of temperatures between 100 K and room temperature. While the CH_2 band splitting, $\Delta\nu_{CH_2}$, is reduced only slightly with increasing temperature (from 13.2 at 100 K to 12.7 cm^{-1} at room temperature), $\Delta\nu_{CD_2}$ is reduced substantially, from 7.9 to 5.0 cm^{-1}, as shown in Figure 13. This decrease corresponds to a decrease in the average size of ordered domains from 10 to 12 to 4−6 chains. However, there is no doubt that the latter figure is an underestimate, since increased temperature also leads to an increase in the cell parameter ratio a/b and to increasing librational amplitude, both of which would cause a reduction in $\Delta\nu_{\infty\times\infty}$. However, the fact that the reduction in $\Delta\nu_{CD_2}$ is much greater than that in $\Delta\nu_{CH_2}$ clearly shows the tendency for thermoreversible surface disordering in annealed crystals.

Another aspect of this equilibrium disordering is revealed by the reversible changes in the absorbance of the conformationally sensitive CH_2 and CD_2 wagging bands. In the CH_2 wagging region the bands of present interest are those at 1367 and 1306 cm^{-1}, characteristic of *gtg* and *gtg′* defects, and the 1352 cm^{-1} band characteristic of *gg* defects.[52] The spectra of $C_{216}H_{385}D_{49}$ in the CH_2 wagging region recorded at 25, 126, and 128 °C (melt) are shown in Figure 14a. Since the alkane $C_{216}H_{385}D_{49}$ is free from CH_3 groups, the spectrum in this region is free from the methyl deformation band at 1378 cm^{-1} which normally interferes with the measurement of the 1367 cm^{-1} band. The temperature dependence of the 1367 and 1352 cm^{-1} absorbances determined by curve fitting is shown in Figure 15. The absorbances have been normalized to their melt values in order to make clear the difference in the melting-induced increase of the two respective types of defects, i.e., *gtg/gtg′* and *gg*. The level of both defects is low and approximately constant up to the melting point. Significantly, the concentration of *gtg/gtg′* defects is 9% of that in the melt, while the equivalent fraction for *gg* defects is only 2%. This can be explained if one assumes that the 1367 cm^{-1} band is mainly due to *gtg′* kink

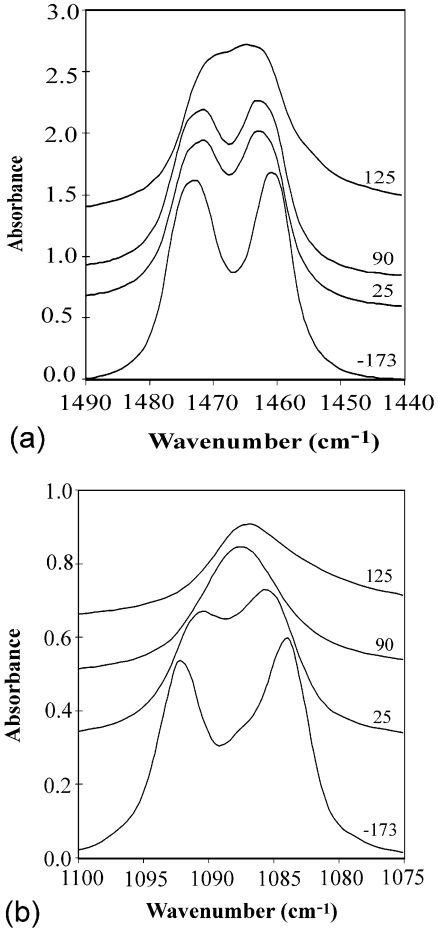

Figure 12. IR spectra of $C_{216}H_{385}D_{49}$ crystals annealed at 125 °C and subsequently recorded in the solid state at the temperatures indicated: (a) CH_2 bending mode, (b) CD_2 bending mode. The reduction in splitting with increasing temperature is more pronounced in (b).

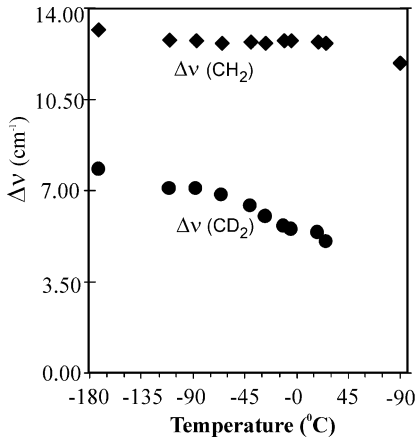

Figure 13. Magnitude of splitting of CH_2 (diamonds) and CD_2 bending modes (circles) for $C_{216}H_{385}D_{49}$ crystals annealed at 125 °C as a function of recording temperature.

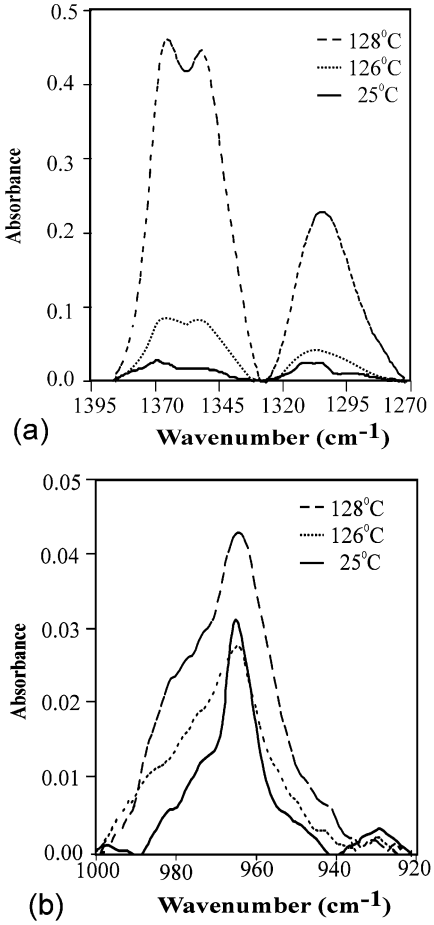

Figure 14. IR spectra of $C_{216}H_{385}D_{49}$ crystals annealed at 125 °C and subsequently recorded at 25, 126, and 128 °C (melt): (a) CH_2 wagging region, (b) CD_2 wagging region. Spectra were normalized against the CH_2 rocking band. Notice the considerably larger increase in CD_2 absorbance, as compared to CH_2 absorbance, in the 126 °C spectrum.

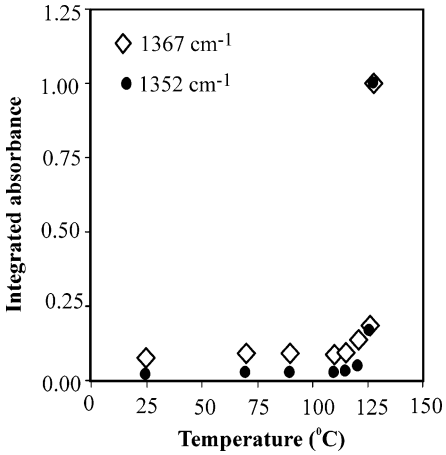

Figure 15. Absorbance of CH_2 wagging bands due to *gtg/gtg′* defects (1367 cm^{-1}) and *gg* defects (1352 cm^{-1}) in annealed $C_{216}H_{385}D_{49}$ crystals as a function of temperature. Normalized to the values for melt at 128 °C. The 1367 cm^{-1} band in the solid is believed to be predominantly due to *gtg′* kink defects.

defects, which leave the chain trajectory straight and can therefore be incorporated within the crystal interior. In contrast to the spectrum of $C_{216}H_{385}D_{49}$, the spectrum of crystalline extended-chain $C_{198}H_{398}$ contains the 1367 and 1352 cm^{-1} bands of nearly equal intensity,[36] confirming that *gg* defects, which bend the chain by 90°, are located almost entirely at the crystal surface. A

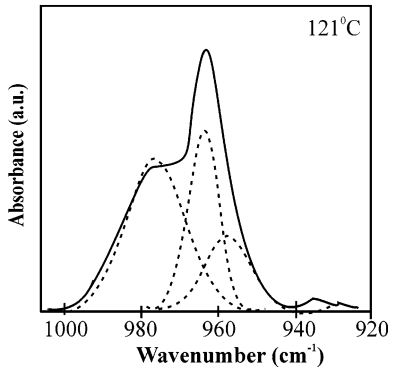

Figure 16. Example of curve resolution into three components in the CD_2 wagging region for $C_{216}H_{385}D_{49}$ crystals at (recorded at 121 °C). The components centered at 976 and 956 cm^{-1} are attributed to conformational defects in deuterated caps[53] and the component at 964 cm^{-1} to CH_2 rocking.[54]

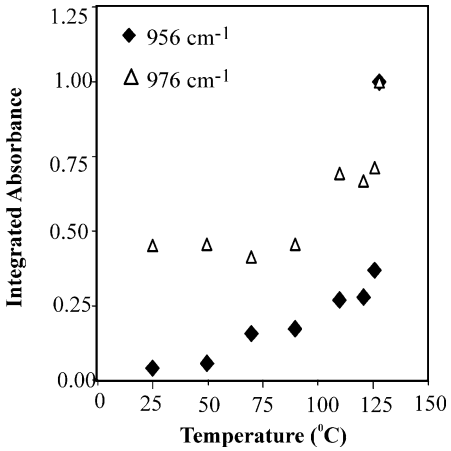

Figure 17. Absorbance of curve-resolved CD_2 defect bands at 956 and 976 cm^{-1} for annealed $C_{216}H_{385}D_{49}$ crystals as a function of temperature. Normalized to the value for melt at 128 °C.

related observation has been made in the study of the orthorhombic−hexagonal transition in irradiated polyethylene,[52] where IR spectra showed a considerable increase in the *gtg/gtg′* band intensity at the transition, with no equivalent increase in the *gg* band.

Unfortunately, mode mixing in deuterated polymethylene chains does not allow such direct association of CD_2 wagging modes with specific conformational defects in the deuterated $C_{12}D_{25}$ caps.[53] Empirically, we find that the greatest effect of crystal melting in the CD_2 wagging region is each side of the band at 964 cm^{-1}, which itself has been attributed to CH_2 rocking.[54] Curve resolution gave the peak frequencies of the two sidebands as 976 and 956 cm^{-1} (see Figure 16). A band at 975 cm^{-1} has been identified previously as a CD_2 wagging mode.[53] Being IR active, it must involve nonplanar conformers. As already mentioned in the previous section, these bands, recorded at room temperature, show an initial decrease in absorbance upon annealing (Figure 11). Figure 17 shows the temperature dependence of normalized intensities of these curve-resolved bands. The 956 cm^{-1} band undergoes a steady increase from 4% to 28% of its melt value between 25 and 121 °C and then triples in intensity at the melting point. Thus, the 956 cm^{-1} band must also be related to conformational defects. The temperature behavior of the two bands would thus indicate a considerable degree of thermal conformational disorder being introduced into

the surface layer prior to melting, in contrast to the small and nearly constant amount of gauche-containing defects in the crystal interior (cf. Figure 15).

Discussion

The main experimental findings can be summarized as follows.

1. Crystallization of alkanes $C_{198}H_{398}$ and $C_{216}H_{385}D_{49}$ from toluene, in both extended and once-folded form, gives crystals with perpendicular chains.

2. In dry crystal mats chain tilt sets in, starting in the range 80−100 °C, and the tilt angle then increases gradually with further increase in temperature, until it reaches 35° close to the melting point. In the case of chain-folded crystals molecules undergo chain extension within the temperature range of increasing tilt.

3. Chain tilting is irreversible.

4. The correlation length of the extended-chain crystals grown from solution is 1300 Å for $C_{216}H_{385}D_{49}$ (1600 Å for $C_{198}H_{398}$ once folded form) and increases greatly (to 7000 Å for $C_{216}H_{385}D_{49}$) just before melting.

5. As judged by the central SAXS scatter, an increase in intercrystalline void content coincides with chain tilting. At higher temperatures effective sintering occurs with the voids removed.

6. In the low-temperature IR spectrum of as-crystallized $C_{216}H_{385}D_{49}$, the Davydov splitting of the CH_2 bending mode, $\Delta\nu_{CH_2}$, is close to its maximum value, indicating large coherently vibrating domains and high molecular order. In contrast, the splitting of the CD_2 mode, $\Delta\nu_{CD_2}$, is considerably smaller, and an additional singlet peak is present between the two crystal components.

7. After annealing at progressively higher temperatures $\Delta\nu_{CD_2}$, measured at low temperature, increases markedly and the area of the singlet decreases by up to 50%.

8. The number of nonplanar conformers in the interior of the as-grown crystals is low and remains low on annealing. In contrast, there is some initial irreversible reduction in conformational disorder at the crystal surface on annealing at $T < 110$ °C, as judged from room temperature spectra in the CD_2 wagging region.

9. With recording temperature increasing from −173 up to 90 °C, using annealed crystals, the CH_2 bending mode splitting $\Delta\nu_{CH_2}$ remains large and changes relatively little (from 14 to 13 cm^{-1}). However, at the same time $\Delta\nu_{CD_2}$ decreases markedly, becoming an unresolved singlet at 90 °C.

10. CH_2 wagging bands, associated with conformational defects *gtg/gtg′* and particularly *gg*, remain low in annealed crystals up to the melting point. In contrast, bands attributed to CD_2 vibrations from conformational defects at the lamellar surface show significant intensity in the solid state, growing steadily and reversibly with increasing temperature.

CH_2 and CD_2 bending mode spectra of the end-deuterated alkane $C_{216}H_{385}D_{49}$ give an interesting picture of the state of order of the crystals as grown from solution. Far from having ordered chain ends, there is a high degree of translational disorder with enough $C_{12}D_{25}$ end groups displaced outside the crystal or into the hydrogenous interior to give rise to a substantial singlet band interposed between the two CD_2 bending components split by crystal field (Figure 9a). Curve fitting gives the ratio of the singlet to the total band area as 0.118, which can be taken as a rough indicator of the fraction of displaced chains. The type of translational disorder in question is schematically illustrated in Figure 18a. A missing deuterated dodecyl group, as far as CD_2 band splitting is concerned, would mean either a vacancy or a "guest" hydrogenous chain, either of which would limit the size of the coupled oscillator domain and thus reduce $\Delta\nu_{CD_2}$. The estimated average domain size of 6−18 chains in as-grown crystals (see above) fits reasonably well with the frequency of chain excursions estimated from the area of the additional singlet.

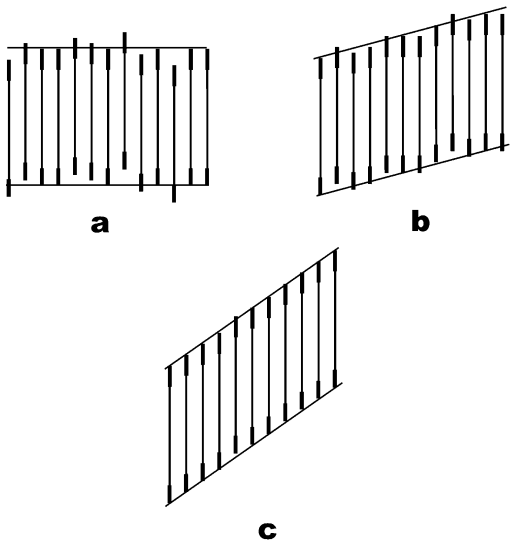

Figure 18. Schematic drawing of molecular arrangements in extended-chain crystals of $C_{216}H_{385}D_{49}$: (a) as grown from solution; (b) annealed at a low temperature−low tilt; (c) annealed at a high temperature−high tilt. Thickened lines indicate deuterated chain ends.

There is even a possibility of the existence of large interlamellar excursions, whereby the deuterated chain end might penetrate the hydrogenous core of the neighboring lamella, passed its deuterated surface layer. There is IR evidence of cilia penetration in mats obtained by slow filtration of mixed suspensions of deuterated and hydrogenous polyethylene single crystals.[55]

It is significant that the decrease in splitting $\Delta\nu_{CD_2}$ and the significant decrease in area of the singlet start only when the annealing temperature exceeds ca. 80 °C (Figure 10), i.e., in the same temperature range in which chain tilt sets in (Figure 3). With temperature increasing further the tilt angle steadily increases, while according to IR evidence, translational disorder steadily decreases. This points to an inverse relationship between translational chain disorder and chain tilt. Three stages of annealing of the solution-crystallized alkane are schematically depicted in Figure 18: (a) as-crystallized, (b) annealed at an intermediate temperature, and (c) annealed just below the melting point.

The above relationship between end group disorder and chain tilt appears to be the exact reverse of the situation in short-chain alkanes. In the closely studied *n*-$C_{33}H_{68}$, for example, chains are perpendicular in the highly ordered low-temperature orthorhombic modification A. At higher temperatures, after two first-order transitions (a layer restacking and a chain shearing transition) a tilted form (C) with {101} basal planes is obtained.[26] The latter structure is attributed to surface roughening, the tilted basal plane providing an enlarged area for the conformationally disordered chain ends.

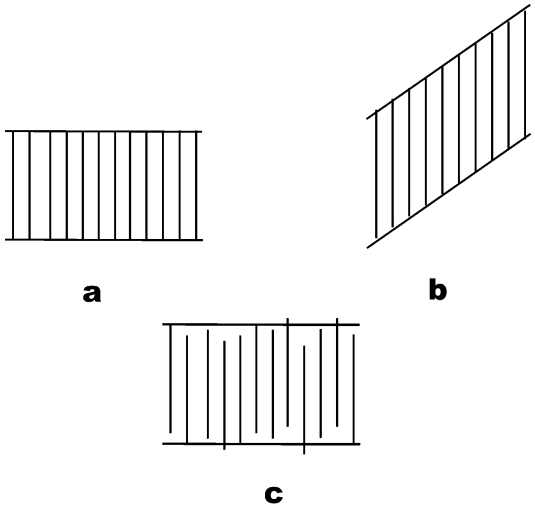

Figure 19. Three situation in crystalline *n*-alkanes (and possibly other chain molecules) regarding chain tilt: (a) pure orthorhombic short alkanes at low temperature—highly order end-surface, perpendicular chains; (b) short or long alkanes and polymers, high temperature—conformationally disordered chain ends, tilted chains; (c) long alkanes and polymers crystallized at low temperature, also impure short alkanes—rough surface (translationally disordered chain ends or folds), perpendicular chains.

Such disordered chain ends have indeed been detected in short *n*-alkanes by IR spectroscopy.[39,51] The lack of tilt in the low-temperature phase of $C_{33}H_{68}$ is thought to be due to the absence of end group disorder (Figure 19a). Even-numbered *n*-alkanes beyond a certain length, such as $C_{36}H_{74}$[56] and $C_{44}H_{90}$,[22] although having {011} basal planes in their ordered low-temperature form, also adopt the {*h*0*l*}-type tilted form close to the melting point, since this allows conformational end group disorder. The tilting transformation produces rooflike ridges along [010],[56] similar to the {310} corrugations in single crystals of polyethylene.[6]

The above comparison with short alkanes can be made more quantitative. We compare the interlayer gap width value D_t, determined by SAXS, for solution-crystalline alkanes $C_{33}H_{68}$ and $C_{216}H_{385}D_{49}$. D_t for the ordered room temperature form A of $C_{33}H_{68}$ has been reported as 1.5 Å,[45] compared with 16 Å found in this work for $C_{216}H_{385}D_{49}$. In comparison, for form C of $C_{33}H_{68}$, measured at 66 °C, D_t is 7.5 Å. Unfortunately, we do not have the D_t value for annealed crystals of $C_{216}H_{385}D_{49}$ at room temperature. It should be noted that the term "interlayer gap" does not imply a layer of air or liquidlike amorphous material, but rather any layer of decreased density, including a less ordered crystal surface.

The question arises as to why crystals with large translational disorder do not require chain tilt, and why tilt is introduced only after the crystal had grown, as the surface smoothens. It is not plausible that chain ends would not require excess volume at temperatures below 80−90 °C where no tilt is observed; the tilted-chain C phase forms in shorter alkanes at even lower temperatures. Furthermore, once tilted, the chains do not revert to perpendicular orientation on cooling. We propose that in as-grown crystals with translational disorder the excess volume is already available to end groups due to their uneven height. In such a crystal (Figure 18a) a buried chain end leaves extra space for the surrounding continuing chains to adopt nonplanar end conformations. However, a crystal of this type has high energy because of large vacancies near the surface. With increasing mobility at elevated temperatures translational order improves and vacancies are eliminated, but a smoother surface brings a reduction in free volume for chain ends. The resulting chain end congestion is then resolved by chain tilt. This would explain the observed inverse relationship between translational chain disorder and chain tilt. Consistent with this interpretation is also the observed initial decrease in the intensities of the 956 and 990 cm^{-1} IR bands on annealing (Figure 11), indicating a decline in nonplanar end group conformers.

The above interpretation is also consistent with the fact that the tilt angle increases gradually with increasing temperature; for the most part the basal plane is not a crystallographic one. On the basis of the behavior of CD_2 bending mode splitting (Figures 9b and 10), we propose that a noncrystallographic basal plane is rough and that the tilt angle is determined by the *average* shear between successive chains, which can locally be either positive or negative (see Figure 18b). The inclination of the surface is determined by the mean displacement. A crystallographic low-index basal plane only makes sense if the surface is reasonably smooth (Figure 18c). The exception is the rough (001) plane in as-grown crystals with orthogonal chains (Figure 18a) where, statistically, the numbers of positive and negative displacements are equal, resulting in zero net shear.

In short-chain *n*-alkanes the basal plane is always crystallographic, and the change from {001} to {101} tilt takes place via a first-order transition. However, as mentioned in the Introduction, when chain length exceeds ca. 50 carbons, tilting is gradual with increasing temperature, as in the current case. The reason for this observation was not understood at the time.[27] According to the present model, this is due to longer chain alkanes crystallizing from solution with a considerable degree of translational disorder. At increasing temperature there is simultaneous gradual surface smoothening and chain tilting. In contrast, short paraffins are unlikely to crystallize with a high degree of translational disorder as the accompanying excess surface energy could not be offset by the bulk crystallization energy of the thin layer interior.

There are in fact two situations in short alkanes where a rough surface does arise and produce an orthogonal crystal where chain tilt might otherwise be expected. Both situations involve even-numbered chains which, in view of the C_{2h} symmetry of the molecule, should not form orthogonal layers.[57] One example is pure even paraffins with more than ca. 30 carbons which, when crystallized rapidly, produce a perpendicular form. Careful annealing or crystallization at a smaller supercooling may produce the stable tilted form with {011} basal planes.[25] The second example are mixed alkanes which most often have perpendicular chains even if the pure components are even-numbered and crystallize with tilted chains.[58] In this case an averaged molecule possesses a mirror plane normal to the chain axis, a symmetry absent in the pure compound. In both cases translational disorder is responsible for the absence of tilt.

The SAXS behavior of once-folded *n*-$C_{198}H_{398}$ is in most respects the same as that of extended-chain $C_{216}H_{385}D_{49}$ and $C_{198}H_{398}$ except for the transformation from folded to extended chains halfway through the

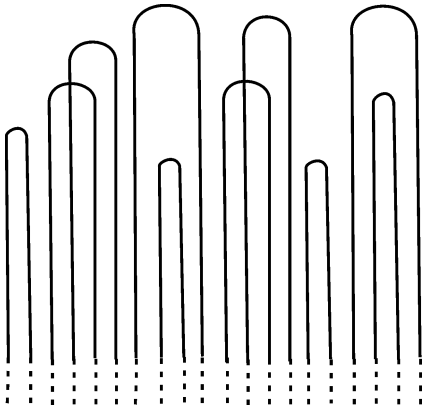

Figure 20. Model of "buried folds" proposed by Sadler.[59]

temperature range of increasing chain tilt (Figures 5 and 6). Therefore, we can conclude that the surface of as-grown chain-folded crystals is also rough and characterized by translational disorder and that it becomes smoother on annealing at elevated temperatures.

Current results support the early suggestion of an initially rough surface in polyethylene single crystals, with ordering and tilting occurring subsequently.[6] At the same time the evidence presented here contradicts the widely held view that perpendicular chains in polymer crystals are due to ordered surfaces. The present work shows a clear difference between kinetic surface disorder, which is largely translational, and the equilibrium thermal disorder, which is primarily conformational. The crystal−amorphous interface is believed to be more diffuse in the as-grown crystals than in those after annealing. The idea of "buried folds" proposed by Sadler[59] as a possible solution to the surface congestion problem (Figure 20) would thus apply to the as-formed crystals grown at low temperatures. The surface overcrowding problem only becomes acute when the surface becomes smoother and it is in response to this that chains tilt. The fold length selection in crystal growth, first discussed by Frank and Tosi,[60] may therefore be a two-stage process at large supercoolings: an initial rough selection, leading to crystals with uneven surfaces, followed by secondary smoothening by solid-state chain diffusion. The idea that perpendicular chain crystals with high translational disorder are less stable but kinetically favored over those with tilted chains is consistent with the recent finding[2,3] that orthogonal crystals grow faster and require a larger supercooling than those with tilted chains.

The reversible equilibrium surface disorder (see Figure 17) is consistent with the reversible increase in SAXS intensity in melt-crystallized long alkanes.[22,42] The presently observed thermal disordering may be compared with the previous IR evidence of temperature-dependent end-gauche content in extended-chain $C_{198}H_{398}$ and chain fold disorder in once-folded $C_{198}H_{398}$ crystals.[36] Current results show a very small and temperature-independent amount of conformational defects in the interior of the crystal layer (Figure 13), a fact that could not be detected previously using all-hydrogenous alkanes or polyethylene. Experimental evidence and theoretical consideration of equilibrium surface disorder are discussed in section II.D of ref 29.

Finally, we comment on the observation in the heating experiments that there is a transient increase in central SAXS scatter coincident with the introduction of chain tilt (Figure 7). We believe that this is due to

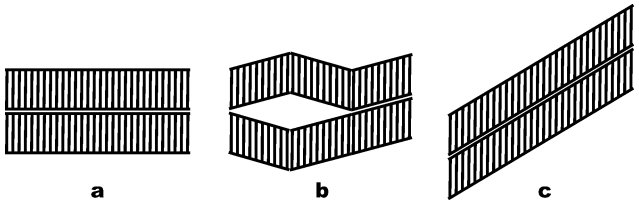

Figure 21. Initial (a), intermediate (b), and final stage of chain tilting (c). The creation of voids in (b) would explain the transient increase in the continuous central SAXS scatter coincident with the largest chain in the tilt angle (cf. Figure 7).

voids forming between lamellae which do not shear in concert with each other (see Figure 21b). Subsequent closing of the voids at higher temperatures suggests that portions of tilted layers may reverse the tilt direction in the process of transforming ridged lamellae into flat ones and eliminating the voids. Close to the melting point large closely packed stacks of parallel lamellae are the result, according to SAXS evidence (the significantly reduced central background and an increased coherence length). Nevertheless, the stacking distortion (g) remains comparatively high.

Acknowledgment. We are greatly indebted to Drs. G. M. Brooke, C. Farren, and A. Harden for the samples of long-chain alkanes. We thank Dr. N. Terrill of Daresbury Synchrotron Laboratory for help in setting up the SAXS experiments on Station 8.2 and Ms. P. A. S. R. Wickramarachchi for the results of experiments on $C_{13}D_{28}$. This work was supported by the Engineering and Physical Science Research Council.

References and Notes

(1) Geil, P. H. *Polymer Single Crystals*; Wiley: New York, 1963.
(2) Keith, H. D.; Padden, F. J. *Macromolecules* **1996**, *24*, 7776.
(3) Abo el Maaty, M. I.; Bassett, D. C. *Polymer* **2001**, *42*, 4957.
(4) Okuda, K.; Yoshida, T.; Sugita, M.; Asahina, M. *J. Polym. Sci., Part A-2* **1967**, *5*, 465.
(5) Briber, R. M.; Khoury, F. *J. Polym. Sci., Part B: Polym. Phys.* **1993**, *31*, 1253.
(6) Bassett, D. C.; Frank, F. C.; Keller, A. *Philos. Mag.* **1963**, *8*, 1753.
(7) Balta Calleja, F. J.; Bassett, D. C.; Keller, A. *Polymer* **1963**, *4*, 269.
(8) Hay, I. L.; Keller, A. *J. Mater. Sci.* **1966**, *1*, 41; **1967**, *2*, 538; **1968**, *3*, 646.
(9) Rognoni, A. F.; Ferracini, E.; Cackovic, J. L.; Cackovic, H. *J. Polym. Sci., Part B: Polym. Phys.* **1984**, *22*, 485.
(10) Khoury, F. *Faraday Discuss. Chem. Soc.* **1979**, *68*, 404.
(11) Bassett, D. C.; Hodge, A. M. *Proc. R. Soc. London A* **1981**, *377*, 25.
(12) Voigt-Martin, I. G. *J. Polym. Sci., Polym. Phys.* **1981**, *19*, 1769.
(13) Frank, F. C. *Discuss. Faraday Soc.* **1979**, *68*, 7.
(14) DiMarzio, E. A.; Guttman, C. M. *Polymer* **1980**, *21*, 733.
(15) Guttman, C. M.; DiMarzio, E. A.; Hoffman, J. D. *Polymer* **1981**, *22*, 1466.
(16) Mansfield, M. L. *Macromolecules* **1988**, *21*, 126.
(17) Balijepalli, S.; Rutledge, G. C. *J. Chem. Phys.* **1998**, *109*, 6523; *Macromol. Symp.* **1998**, *133*, 71.
(18) Lovinger, A. J.; Keith, H. D. *Macromolecules* **1996**, *29*, 8541.
(19) Gautam, S.; Balijepalli, S.; Rutledge, G. C. *Macromolecules* **2000**, *33*, 9136.
(20) Zeng, X. B.; Ungar, G. *Macromolecules* **2001**, *34*, 6945.
(21) Toda, A.; Arita, T.; Hikosaka, M. *Polymer* **2001**, *42*, 2223.
(22) Sullivan, P. K.; Weeks, J. J. *J. Res. Natl. Bur. Stand. A* **1970**, *74*, 203.
(23) Ungar, G.; Stejny, J.; Keller, A.; Bidd, I.; Whiting, M. C. *Science* **1985**, *229*, 386.
(24) Smith, A. E. *J. Chem. Phys.* **1953**, *21*, 2229.
(25) Shearer, H. M. M.; Vand, V. *Acta Crystallogr.* **1956**, *9*, 379.
(26) Piesczek, W.; Strobl, G. R.; Malzahn, K. *Acta Crystallogr., Sect. B* **1974**, *30*, 1278.

(27) Takamizawa, K.; Ogawa, Y.; Oyama, T. *Polym. J.* **1982**, *14*, 441.
(28) Reneker, D. H.; Geil, P. H. *J. Appl. Phys.* **1960**, *31*, 1916.
(29) Ungar, G.; Zeng, X. B. *Chem. Rev.* **2001**, *101*, 4157.
(30) Winkel, A. K.; Hobbs, J. K.; Miles, M. J. *Polymer* **2000**, *41*, 8791.
(31) Hosier, I. L.; Bassett, D. C.; Vaughan, A. S. *Macromolecules* **2000**, *33*, 8781.
(32) Ungar, G.; Putra, E. G. R. *Macromolecules* **2001**, *34*, 5180.
(33) Zeng, X. B.; Ungar, G.; Spells, S. J. *Polymer* **2000**, *41*, 8775.
(34) Zeng, X. B.; Ungar, G. *Phys. Rev. Lett.* **2001**, *86*, 4875; *Macromolecules* **2001**, *34*, 6945; *Polymer* **2002**, *43*, 1657.
(35) Ungar, G.; Mandal, P.; Higgs, P. G.; de Silva, D. S. M.; Boda, E.; Chen, C. M. *Phys. Rev. Lett.* **2000**, *85*, 4397.
(36) Ungar, G.; Organ, S. J. *Polym. Commun.* **1987**, *28*, 232.
(37) Brooke, G. M.; Burnett, S.; Mohammed, S.; Proctor, D.; Whiting, M. C. *J. Chem. Soc., Perkin Trans. 1* **1996**, 1635.
(38) Brooke, G. M.; Farren, C.; Harden, A.; Whiting, M. C. *Polymer* **2001**, *42*, 2777.
(39) Zerbi, G.; Magni, R.; Gussoni, M.; Holland-Moritz, K.; Bigotto, A.; Dirlikov, S. *J. Chem. Phys.* **1981**, *75*, 3175.
(40) Broadhurst, M. G. *J. Res. Natl. Bur. Stand. A* **1962**, *66*, 241.
(41) Ungar, G.; Organ, S. J.; Keller, A. *J. Polym. Sci., Part C: Polym. Lett.* **1988,** *26*, 259.
(42) Zeng, X. B.; Ungar, G. *Polymer* **1998**, *39*, 4523.
(43) Hosemann, R.; Bagchi, S. N. *Direct Analysis of Diffraction by Matter*; North-Holland: Amsterdam, 1962.
(44) de Silva, D. S. M.; Gorce, J.-P.; Wickramarachchi, P. A. S. R.; Spells, S. J. *Macromol. Symp.*, submitted for publication.
(45) Strobl, G.; Ewen, B.; Fischer, E. W.; Piesczek, W. *J. Chem. Phys.* **1974**, *61*, 5257.
(46) Zbinden, R. *Infrared Spectroscopy of High Polymers*; Academic Press: New York, 1964.
(47) Cheam, T. C.; Krimm, S. *J. Polym. Sci., Polym. Phys. Ed.* **1981**, *19*, 423.
(48) Spells, S. J. In *Characterization of Solid Polymers*; Spells, S. J., Ed.; Chapman and Hall: London, 1994; pp 166−223.
(49) Spells, S. J. *Polymer* **1985**, *26*, 1921. Coutry, S.; Spells, S. J., submitted to *Polymer*.
(50) Ungar, G.; Masic, N. *J. Phys. Chem.* **1985**, *89*, 1036.
(51) Maroncelli, M.; Qi, S. P.; Strauss, H. L.; Snyder, R. G. *J. Am. Chem. Soc.* **1982**, *104*, 6237.
(52) Ungar, G. *Macromolecules* **1986**, *19*, 1317.
(53) Hirata, S.; Iwata, S. *J. Chem. Phys.* **1998**, *108*, 7901.
(54) Krimm, S.; Liang, C. Y.; Sutherland, G. B. B. M. *J. Chem. Phys.* **1956**, *25*, 549.
(55) Bank, M. I.; Krimm, S. *J. Appl. Phys.* **1969**, *40*, 4248.
(56) Keller, A. *Philos. Mag.* **1961**, *6*, 329.
(57) Kitaigorodskii, A. *Organic Chemical Crystallography*; Consultants Bureau: New York, 1961.
(58) Rajabalee, F.; Metivaud, V.; Mondieig, D.; Haget, Y.; Cuevas-Diarte, M. A. *J. Mater. Res.* **1999**, *14*, 2644.
(59) Sadler, D. M. *Faraday Discuss. Chem. Soc.* **1979**, *68*, 106.
(60) Frank, F. C.; Tosi, M. *Proc. R. Soc. London A* **1961**, *263*, 323.

MA0206669